Monthly Notices
of the
ROYAL ASTRONOMICAL SOCIETY

Mon. Not. R. Astron. Soc. **414,** 1032–1046 (2011) doi:10.1111/j.1365-2966.2011.18410.x

Effect of foregrounds on the cosmic microwave background radiation multipole alignment

Pavan K. Aluri,[1] Pramoda K. Samal,[2] Pankaj Jain[1]★ and John P. Ralston[3]

[1]*Department of Physics, Indian Institute of Technology, Kanpur 208016, India*
[2]*Department of Physics, Utkal University, Bhubaneswar 751004, India*
[3]*Department of Physics and Astronomy, University of Kansas, Lawrence, KS 66045, USA*

Accepted 2011 January 23. Received 2010 November 30; in original form 2010 July 15

Downloaded from https://academic.oup.com/mnras/article/414/2/1032/976641 by guest on 31 July 2023

ABSTRACT

We analyse the effect of foregrounds on the observed alignment of the cosmic microwave background radiation (CMBR) quadrupole and octopole. The alignment between these multipoles is studied by using a symmetry-based approach which assigns a principal eigenvector (PEV) or an axis with each multipole. We determine the alignment between these multipoles and its significance using the internal linear combination (ILC) 5- and 7-yr maps. We also use the maps obtained by applying the internal power spectrum estimation (IPSE) procedure on the corresponding *Wilkinson Microwave Anisotropy Probe* data sets to assess its significance. The effect of foreground cleaning is studied in detail within the framework of the IPSE method both analytically and numerically. By using simulated CMBR data, including foregrounds and detector noise, we study how the PEVs of the simulated pure CMB maps differ from those of the corresponding clean maps. We find that, in general, the shift in the PEVs is relatively small and in random directions. Because of the random nature of the shift we conclude that the residual foregrounds can only lead to misalignment rather than cause alignment of multipoles. We also directly estimate the significance of the observed alignment by using simulated clean maps. We find that the results in this case are identical to those obtained by simple analytic estimates or by using simulated pure CMB maps.

Key words: methods: data analysis – methods: statistical – cosmic background radiation.

1 INTRODUCTION

The standard cosmological model rests on the *cosmological principle* which states that the Universe is homogeneous and isotropic. However, there are many indications from diverse data sets that this principle may not be applicable. In particular, polarizations of radio waves coming from distant radio galaxies (Birch 1982; Jain & Ralston 1999), the optical polarizations from quasars (Hutsemékers 1998; Hutsemékers & Lamy 2001; Jain, Narain & Sarala 2004) and the multipoles $l = 1, 2, 3$ of cosmic microwave background radiation (CMBR) all indicate a universal axis pointing in the direction of the Virgo cluster (de Oliveira-Costa et al. 2004; Ralston & Jain 2004; Schwarz et al. 2004). This phenomenon has been called the *Virgo alignment puzzle* (Ralston & Jain 2004). There have also been other claims of large-scale anisotropy in the CMBR data. These include the dipole power modulation (Eriksen et al. 2004, 2007b; Hoftuft et al. 2009), the detection of an anomalously cold spot (Cruz et al. 2005), as well as an anomalous signal in the ecliptic plane (Diego et al. 2010). These and many other CMB anomalies have been studied in great detail (Bielewicz, Górski & Banday 2004; Hansen, Banday & Górski 2004; Katz & Weeks 2004; Bielewicz et al. 2005; Prunet et al. 2005; Bernui et al. 2006, 2007; Copi et al. 2006, 2007; de Oliveira-Costa & Tegmark 2006; Freeman et al. 2006; Helling, Schupp & Tesileanu 2006; Wiaux et al. 2006; Land & Magueijo 2007; Magueijo & Sorkin 2007; Vielva et al. 2007). Meanwhile, some studies did not find any violation of statistical isotropy in the CMB (Hajian, Souradeep & Cornish 2004; Hajian & Souradeep 2006). Furthermore, the cluster peculiar velocities (Kashlinsky et al. 2008, 2009), as well as the large-scale galaxy distribution (Itoh, Yahata & Takada 2010), also indicate deviations from isotropy. The preferred axis for the cluster peculiar velocities with a high-redshift cut is found to be again close to the direction of the Virgo cluster. In the galaxy distribution surveys, the preferred axis appears to depend strongly on the cut made on the data.

There have been a variety of proposals in the literature discussing the possible origin of this *alignment anomaly*, such as anisotropic space–times (Berera, Buniy & Kephart 2004; Kahniashvili, Lavrelashvili & Ratra 2008), foreground contaminations (Slosar & Seljak 2004;

★E-mail: pkjain@iitk.ac.in

© 2011 The Authors
Monthly Notices of the Royal Astronomical Society © 2011 RAS

Abramo, Sodre & Wuensche 2006; Rakić, Rasanen & Schwarz 2006), noise bias or systematics (Gruppuso, Burigana & Finelli 2007; Naselsky, Verkhodanov & Nielsen 2008), vector-like dark energy (Armendariz-Picon 2004), spontaneous breaking of isotropy (Gordon et al. 2005; Land & Magueijo 2006; Erickcek, Hirata & Kamionkowski 2009), inhomogeneous universe (Moffat 2005; Land & Magueijo 2006), inhomogeneous inflation (Carroll, Tseng & Wise 2010), violation of rotational invariance during inflation (Ackerman, Carroll & Wise 2007), anisotropic perturbations due to dark energy (Battye & Moss 2006), anisotropic inflation (Buniy, Berera & Kephart 2006), local voids (Inoue & Silk 2006) and anisotropic dark energy (Koivisto & Mota 2008; Rodrigues 2008).

Another interesting effect associated with the quadrupole is its low power in comparison to the best-fitting Λ cold dark matter (ΛCDM) model (Bennett et al. 2003a). One may speculate that the observed quadrupole–octopole alignment is related to the observed low quadrupole power. It has been shown that in random realizations of pure CMB maps there is no correlation between the low quadrupole power and quadrupole–octopole alignment (Rakić & Schwarz 2007; Sarkar et al. 2010).

In the present paper, we analyse the alignment of CMBR quadrupole ($l = 2$) and octopole ($l = 3$) moments more closely. In Slosar & Seljak (2004), it has been suggested that this alignment may be caused by the galactic foregrounds. These authors argue that most of the power of the quadrupole and octopole lies in the most contaminated region of the sky. Hence, it is entirely possible that these multipoles may be significantly contaminated and the alignment may be caused due to poor cleaning. The internal linear combination (ILC) map, provided by the *Wilkinson Microwave Anisotropy Probe* (*WMAP*) team (Bennett et al. 2003b), as revised in Gold et al. (2009), has been found to be consistent with Gaussian random realizations (Gruppuso & Burigana 2009) and hence may not be significantly contaminated. However, according to the authors, this still does not rule out the possibility that it may be contaminated with a residual which follows a Gaussian distribution.

In the internal power spectrum estimation (IPSE) procedure (Saha, Jain & Souradeep 2006; Saha et al. 2008; Samal et al. 2010), the cleaning is performed by a blind procedure without making any explicit model for foregrounds. The foregrounds are removed by adding maps in harmonic space at different frequencies with suitable weights, chosen so as to minimize the foreground power. There also exist other blind procedures, applicable at low l, for foreground cleaning (Tegmark & Efstathiou 1996; Maino et al. 2002; Martínez-González et al. 2003; Tegmark, de Oliveira-Costa & Hamilton 2003; Hansen et al. 2006; Eriksen et al. 2007a, 2008). Some of these are reviewed in Leach et al. (2008). The ILC map is also obtained by using a blind cleaning procedure (Bennett et al. 2003b). Here the weighted maps are added directly in pixel space. Both the IPSE and ILC procedures are highly effective in removing foregrounds. However, some residual foregrounds may still contaminate the data. Besides this, Saha et al. (2008) and Samal et al. (2010) pointed out the existence of a bias in the low-l multipoles extracted from foreground cleaned maps. This bias leads to a significant reduction of extracted power in these multipoles. Hence it might provide a consistent explanation of the observed low power at $l = 2$, in comparison to the best-fitting theoretical ΛCDM model. It is clearly important to determine what this low-l bias might imply for the alignment of these multipoles. It could be that the power gets eliminated in just the precise manner in order to cause alignment. Here we study whether any of these residuals present in the foreground cleaned data may cause the observed quadrupole–octopole alignment.

It is important to note that the observed alignment is only getting better with more data. A larger data sample implies smaller uncertainties due to detector noise. Hence, the signal becomes more prominent as the fluctuations due to detector noise get suppressed. It will, therefore, be very interesting to see how the signal changes with more data from *WMAP* and *Planck* (Planck Collaboration 2005; Lamarre et al. 2010; Mandolesi et al. 2010; Tauber et al. 2010).

The problem of testing violation of isotropy in the CMBR signal has been addressed by many authors. The CMBR anisotropy spectrum is generally assumed to be isotropic in a statistical sense. We can make a spherical harmonic expansion of CMBR anisotropies observed over the sky as

$$\Delta T(\theta, \phi) = \sum_{l=0}^{\infty} \sum_{m=-l}^{+l} a_{lm} Y_{lm}(\theta, \phi), \tag{1}$$

where θ and ϕ are the usual spherical polar coordinates. Thus, the assumption of statistical isotropy of the CMBR signal means that the spectral coefficients, a_{lm}, are uncorrelated for different m and l, i.e. the ensemble average,

$$\langle a^*_{lm} a_{l'm'} \rangle = \delta_{ll'} \delta_{mm'} C_l, \tag{2}$$

where C_l is the standard power. A multitude of statistics have been proposed in order to test for deviation from statistical isotropy in the CMBR data (Hajian et al. 2004; Bernui et al. 2006; Copi et al. 2006, 2007; Hajian & Souradeep 2006). Here, we shall use the method introduced in Ralston & Jain (2004) and further developed in Samal et al. (2008, 2009). In this procedure, we construct what we call a 'power tensor' for each multipole using the spectral coefficients, a_{lm}, and generators of the SO(3) rotation group. Then, one assigns three orthogonal unit vectors for each multipole extracted from this power tensor. The orientation of these vectors, as well as the power associated with each vector, contains information about possible violation of statistical isotropy. This information is encoded in two entropy measures, the power entropy and alignment entropy, defined in Samal et al. (2008). Using this method one can test for violation of isotropy for each individual multipole or collectively over a range of multipoles. We present an outline of our analysis procedure in Section 2, with results from cosmological data and simulations in Section 3 and, finally, summarize our conclusions in Section 4.

Downloaded from https://academic.oup.com/mnras/article/414/2/1032/976641 by guest on 31 July 2023

2 ANALYSIS METHODOLOGY

The primary objective of the present paper is to determine whether the alignment of quadrupole and octopole can be caused by foreground contamination. The alignment of different multipoles can be quantified by associating a frame with each multipole (Ralston & Jain 2004; Samal et al. 2008). In order to analyse the effect of foreground contamination we first perform an analytic calculation of the power tensor, introduced in Ralston & Jain (2004) and Samal et al. (2008), within the framework of the IPSE technique (Saha et al. 2006, 2008; Samal et al. 2010). Here we confine ourselves to the simple case of one foreground component following rigid frequency scaling and two frequency bands. This computation is useful to determine if the low-l bias (Saha et al. 2008; Samal et al. 2010) also leads to violation of statistical isotropy. We then numerically determine the effect of this bias and residual foregrounds on the alignment of quadrupole and octopole. We generate many random realizations of the CMBR maps and add foregrounds and detector noise to them. We use the *Planck* Sky Model (PSM)[1] for foregrounds and use all the five *WMAP* frequency bands in our analysis. These simulated raw maps are cleaned using the IPSE technique. We study the difference in the extracted principal eigenvectors (PEVs) of clean maps and simulated pure CMB maps. This allows us to determine if the residual foregrounds lead to any preferential alignment of these vectors. In the next subsections, we briefly review the extraction of frames and the IPSE technique.

2.1 Covariant frames

The present study utilizes a symmetry-based statistic (Samal et al. 2008) to test for statistical isotropy in the CMBR data. The method associates a wavefunction, ψ^k_m, defined as

$$\psi^k_m(l) = \frac{1}{\sqrt{l(l+1)}} \langle l, m | J^k | a(l) \rangle \tag{3}$$

with every multipole l. Here $|a(l)\rangle$ contains information about the spectral moments, such that

$$a_{lm} = \langle l, m | a(l) \rangle, \tag{4}$$

where $|lm\rangle$ are the eigenstates of the angular momentum operators $\boldsymbol{J}^2, J_z$ in the spin l representation. The wavefunction ψ^k_m is useful since it assigns a frame, i.e. three orthonormal vectors, at each l. The frame can be extracted by making a singular value decomposition (SVD) of the wavefunction. This assigns the singular values Λ^α and two frames e^α_k and u^α_m for each l (Ralston & Jain 2004) as

$$\psi^k_m = \sum_{\alpha=1}^{3} e^\alpha_k \Lambda^\alpha u^{\alpha *}_m. \tag{5}$$

Here the indices, $\alpha = 1, 2, 3$, $k = 1, 2, 3$ and $m = -l, \ldots, +l$. Here we are interested in the orientation of any particular multipole in real space. This information is contained in the frames e^α_k. The relationship of the wavefunction ψ^k_m to the Maxwell multipole vectors (Copi et al. 2006, 2007) is discussed in Samal et al. (2008).

It is also convenient to define the 'power tensor' (Ralston & Jain 2004; Samal et al. 2008),

$$\begin{aligned} \mathcal{A}_{ij}(l) &= \sum_m \psi^i_m \psi^{j\,*}_m \\ &= \frac{1}{l(l+1)} \sum_{m,m'} a^*_{lm} (J_i J_j)_{mm'} a_{lm'}. \end{aligned} \tag{6}$$

The frame associated with each multipole e^α_i, $\alpha = 1, 2, 3$, consists of the three eigenvectors of this matrix. The index, $i = 1, 2, 3$, labels the three components of each eigenvector. The corresponding eigenvalues, $(\Lambda^\alpha)^2$, contain information about the power associated with each eigenvector. The sum of the three eigenvalues equals the total power, C_l. A large dispersion in the eigenvalues indicates violation of statistical isotropy for a particular mode. For example, if only one of the eigenvalues is non-zero that would imply that the particular mode is maximally anisotropic. The eigenvector corresponding to that eigenvalue would define the preferred direction in real space.

The above discussion leads us to define the PEV, $\hat{n}_l$, as the eigenvector corresponding to the maximum eigenvalue (Ralston & Jain 2004; Samal et al. 2008). In the case of low l that we studied here, the largest eigenvalue generally carried at least 65 per cent of the total power, C_l, in each l. We note that the extracted PEVs are headless, meaning, these vectors specify only an axis and not a direction. As explained in Ralston & Jain (2004), the PEV is analogous to the preferred axis extracted in de Oliveira-Costa et al. (2004). The P value or the significance of alignment between the quadrupole and octopole PEVs can be estimated analytically by the formula $P = 1 - \hat{n}_2 \cdot \hat{n}_3 = 1 - \cos(\delta\Theta)$. Here $\delta\Theta$ is the angle between the two PEVs $\hat{n}_2$ and $\hat{n}_3$, which correspond to $l = 2$ and 3, respectively. Alternatively, one can estimate the significance directly by numerical simulations, as described below.

2.2 IPSE method

The IPSE procedure (Saha et al. 2006, 2008; Samal et al. 2010) removes the foreground contamination by linearly combining maps at different frequencies with suitable weights in harmonic space. The cleaning is accomplished independently for each l. Let $\hat{w}^a_l$ denote the weights for

[1] http://www.planck.fr/heading79.html

Downloaded from https://academic.oup.com/mnras/article/414/2/1032/976641 by guest on 31 July 2023

the map at frequency channel a corresponding to the multipole l. In case we have several maps at a particular frequency, we simply take their average. The spherical harmonic components of the cleaned map are given by

$$a_{lm}^{\rm Clean} = \sum_{a=1}^{n_{\rm c}} \hat{w}_l^a \frac{a_{lm}^a}{B_l^a}. \tag{7}$$

Here $n_{\rm c}$ is the total number of frequency channels used for cleaning. The factor B_l^a is the circularized beam transform function at frequency band a (Hill et al. 2009). The a_{lm}^a represents the harmonic coefficients of the observed map. It can be expressed as

$$a_{lm}^a = \left(a_{lm}^s + a_{lm}^{(f)a}\right) B_l^a + a_{lm}^{(N)a}, \tag{8}$$

where a_{lm}^s, $a_{lm}^{(f)a}$ and $a_{lm}^{(N)a}$ represent the contributions from CMB, foregrounds and detector noise, respectively, at frequency channel a.

The weights $\hat{w}_l^a$ are obtained by minimizing the total power subject to the constraint

$$\hat{\mathbf{W}}_l \mathbf{e}_0 = \mathbf{e}_0^{\rm T} \hat{\mathbf{W}}_l^{\rm T} = 1, \tag{9}$$

where $\mathbf{e}_0$ is a column vector with unit elements,

$$\mathbf{e}_0 = \begin{pmatrix} 1 \\ .. \\ .. \\ 1 \end{pmatrix}, \tag{10}$$

and $\hat{\mathbf{W}}_l$ is the row vector $(\hat{w}_l^1, \hat{w}_l^2, \ldots, \hat{w}_l^{n_{\rm c}})$. This gives

$$\hat{\mathbf{W}}_l = \frac{\mathbf{e}_0^{\rm T} \hat{\mathbf{C}}_l^{-1}}{\mathbf{e}_0^{\rm T} \hat{\mathbf{C}}_l^{-1} \mathbf{e}_0}, \tag{11}$$

where $\hat{\mathbf{C}}_l$ is the empirical covariance matrix (Tegmark & Efstathiou 1996; Tegmark et al. 2003; Saha et al. 2006; Delabrouille & Cardoso 2009). Its ab matrix element may be expressed as, $\hat{C}_l^{ab}/(B_l^a B_l^b)$, where $\hat{C}_l^{ab}$ is the cross power spectrum between the ath and bth channel,

$$\hat{C}_l^{ab} = \sum_{m=-l}^{m=l} \frac{a_{lm}^a a_{lm}^{b*}}{2l+1}. \tag{12}$$

The final cleaned map may be used to extract the power spectrum as well as the PEVs needed for the present study. The power spectrum is given by

$$\hat{C}_l^{\rm Clean} = \frac{1}{\mathbf{e}_0^{\rm T} \hat{\mathbf{C}}_l^{-1} \mathbf{e}_0}. \tag{13}$$

This would be reliable at low l, where the detector noise is negligible. For our present purpose, this is sufficient. However at high $l > 200$, where the detector noise is not negligible, a more elaborate procedure is necessary, as discussed in Saha et al. (2006, 2008).

The procedure contains some bias which can be estimated from simulations. An important bias arises due to inefficient cleaning in the galactic plane. A similar bias is also present in the procedure used by the *WMAP* science team in generating the ILC map. As a final step in generating this map, a 'bias' correction based on Monte Carlo simulations is applied by the *WMAP* science team (Hinshaw et al. 2007). We employ a similar procedure to correct for any residual foreground bias by subtracting a 'bias map' generated from the simulated maps in pixel space.

Another interesting bias arises due to the cross-correlation term between the foregrounds and the CMB signal in the estimation of CMB power. This bias is negative and affects dominantly the very low multipoles. This can also be estimated by simulations, but may also be represented analytically by using some simplifying assumptions (Saha et al. 2008).

2.3 Simulations

In order to study the effect of foregrounds on the detected anisotropy in the CMBR, we generate an ensemble of 500 CMB maps as random realizations of the best-fitting theoretical power spectrum, available at the NASA's *WMAP* public domain webpage.[2] These simulated 'pure' CMB maps are generated using the publicly available HEALPIX software.[3] These 'pure maps' are generated at resolution 9 ($N_{\rm side} = 512$) of the HEALPIX sky pixelization scheme. We perform our entire analysis at this resolution. We are interested only in the alignment of the $l = 2$, 3 multipoles. Hence we do not expect our results to depend on the adopted resolution. Some of the statistical analysis used to quantify the low l anomalies, such as alignment of $l = 2$, 3 multipoles, have been performed earlier (Bernui et al 2006, 2007; Hansen et al. 2006, 2009; Wiaux et al 2006; Vielva et al 2007), using sky maps at lower resolution, such as $N_{\rm side} = 16$, 32, 128, 256. The significance of results obtained by these authors is not significantly different from that obtained at higher resolution. Hence our results are expected to be independent of the adopted resolution of the sky maps.

[2] http://lambda.gsfc.nasa.gov/
[3] http://healpix.jpl.nasa.gov/

© 2011 The Authors, MNRAS **414,** 1032–1046
Monthly Notices of the Royal Astronomical Society © 2011 RAS

Downloaded from https://academic.oup.com/mnras/article/414/2/1032/976641 by guest on 31 July 2023

After extracting the PEVs of these pure maps, we contaminate the maps with galactic foregrounds and also add Gaussian random noise with appropriate dispersion per pixel. We use PSM templates as our all-sky foreground maps. The foregrounds included in PSM are thermal dust, synchrotron and free–free galactic emission templates only. These are the dominant foregrounds as characterized by the *WMAP* science team also in all its data releases so far (Gold et al. 2011). The effective number of observations, $N_{\rm obs}$, needed to generate the noise maps is obtained from the temperature maps of *WMAP* 5 and 7 year data sets, along with σ_0, which are available in FITS format at NASA's LAMBDA website.[2] The effective noise per pixel is given by $\sigma = \sigma_0/\sqrt{N_{\rm obs}}$. These simulated CMB maps are then passed through a cleaning pipeline which uses the IPSE procedure to clean the maps. This produces a full sky cleaned map corresponding to each random realization which can be used to study the alignment between quadrupole and octopole. By comparing observations with the random samples, we can easily estimate the significance level of the observed alignment. Furthermore, we can study how the PEVs in the extracted clean CMB maps differ from those of pure CMB maps. This can reveal any systematic bias which may be present in the PEVs of cleaned maps. Because of the presence of residual foregrounds and negative bias at low l, we expect that the corresponding eigenvectors may also be biased. Here we shall study this bias and its effect on alignment of quadrupole and octopole.

Besides the dominant foregrounds mentioned above, many authors have reported the existence of some subdominant or not yet fully understood foregrounds like, for example, spinning dust grains, dust components correlated with synchrotron (Kogut et al. 1996; Bennett et al. 2003b; Dobler & Finkbeiner 2008b), foreground *X* (de Oliveira-Costa et al. 2002), an anomalous emission component in *WMAP* data (Bonaldi et al. 2007), an anomalous haze component (Dobler & Finkbeiner 2008a) and spuriously large galactic synchrotron emission in *WMAP* data (La Porta et al. 2008) compared to a simple extrapolation of microwave flux from the 408 MHz (Haslam et al. 1982) and 1.42 GHz (Reich & Reich 2008) all-sky maps. Dobler & Finkbeiner (2008b) also mention the presence of a spinning dust component at roughly 20 per cent of the level of usual foregrounds. However there is considerable uncertainty in these subdominant foreground components and a consistent model is still elusive (Gold et al. 2011).

The simulations were run on an Intel(R) Xenon(R) CPU cluster with 2 Quad Core processors @2.50 GHz and 16 MB RAM. It took about 2 d to complete the pipeline which includes generating 500 pure CMB maps, cleaning the foreground and noise contaminated maps and finally extracting the eigenvalues and eigenvectors of the power tensor thus constructed for each map.

3 EFFECT OF LOW-L BIAS

In this section we evaluate analytically how the low-l negative bias, arising due to chance correlation between CMB signal and foregrounds, affects the power tensor. For simplicity we assume that there is only one significant foreground component, which follows rigid frequency scaling. Furthermore, we assume only two frequency bands in the CMB data analysis. The detector noise is assumed to be negligible, which is a reasonable assumption at low l. For simplicity we also set the beam transform function to unity. We compute the ensemble average of the power tensor within the framework of the IPSE method using these simplifying assumptions.

The wavefunction $\psi^i_m(l)$ associated with each multipole, equation (3), may be expressed as

$$\psi^i_m(l) = \frac{1}{\sqrt{l(l+1)}} \sum_{m'} \langle lm|J_i|lm'\rangle a_{lm'}. \tag{14}$$

The corresponding power tensor may be written as

$$\mathcal{A}_{ij}(l) = \frac{1}{l(l+1)} \sum_{m,m',m''} \langle lm|J_i|lm'\rangle \langle lm''|J_j|lm\rangle a_{lm'} a^*_{lm''}. \tag{15}$$

To calculate the bias in the power tensor we take its ensemble average to get

$$\langle \mathcal{A}_{ij}(l)\rangle_{\rm ens.avg.} = \frac{1}{l(l+1)} \sum_{m,m',m''} \langle lm|J_i|lm'\rangle \langle lm''|J_j|lm\rangle \langle a_{lm'} a^*_{lm''}\rangle_{\rm ens.avg.}, \tag{16}$$

where the symbol $\langle\rangle_{\rm ens.avg.}$ denotes ensemble average. It follows from the *cosmological principle* that the fluctuations in CMBR are statistically isotropic. Hence we expect for a pure CMB map

$$\langle \mathcal{A}_{ij}(l)\rangle_{\rm ens.avg.} = \frac{C_l}{3}\delta_{ij}. \tag{17}$$

Here we compute the ensemble average of the power tensor for the cleaned map. This will show us whether the bias generated due to foreground cleaning leads to anisotropy in the power tensor.

The spherical harmonic coefficients of a cleaned map can be written as

$$a^{\rm Clean}_{lm} = a^{(s)}_{lm} + a^{\rm res}_{lm}, \tag{18}$$

where $a^{\rm res}_{lm}$ denotes any residual foreground contamination in the cleaned map,

$$a^{\rm res}_{lm} = \sum_{b=1}^{n_{\rm c}} \hat{w}^b_l a^{(f)b}_{lm}. \tag{19}$$

Downloaded from https://academic.oup.com/mnras/article/414/2/1032/976641 by guest on 31 July 2023

In order to estimate the bias in the power tensor, we need to calculate

$$\begin{aligned}\left\langle a_{lm'}^{\rm Clean} a_{lm''}^{\rm Clean*}\right\rangle_{\rm ens.avg.} &= \left\langle \left(a_{lm'}^{(s)} + \sum_{b=1}^{n_{\rm c}} \hat{w}_l^b a_{lm'}^{(f)b}\right)\left(a_{lm''}^{(s)} + \sum_{b'=1}^{n_{\rm c}} \hat{w}_l^{b'} a_{lm''}^{(f)b'}\right)^* \right\rangle \\ &= C_l^{(s)}\delta_{m'm''} + \left\langle a_{lm'}^{(s)} \hat{w}_l^{b'} a_{lm''}^{(f)b'*}\right\rangle + \left\langle a_{lm''}^{(s)\,*} \hat{w}_l^{b} a_{lm'}^{(f)b}\right\rangle + \left\langle \hat{w}_l^{b} a_{lm'}^{(f)b} a_{lm''}^{(f)b'*} \hat{w}_l^{b'}\right\rangle. \end{aligned} \tag{20}$$

The first term after the second equality follows from the assumption that CMB signal is statistically isotropic. The frequency band indices b and b' in the second, third and fourth terms are summed over as in the Einstein summation convention.

The elements of the empirical covariance matrix are given by

$$\begin{aligned}\hat{C}_l^{ab} &= \frac{1}{2l+1}\sum_{m=-l}^{+l} a_{lm}^a a_{lm}^{b*} \\ &= \frac{1}{2l+1}\sum_{m=-l}^{+l}\left(a_{lm}^{(s)} + a_{lm}^{(f)a}\right)\left(a_{lm}^{(s)} + a_{lm}^{(f)b}\right)^* \\ &= \hat{C}_l^{(s)} + \hat{C}_l^{(s)(f)a} + \hat{C}_l^{(s)(f)b} + C_l^{(f)a(f)b}. \end{aligned} \tag{21}$$

Terms in the last line correspond to each of the cross-multiplication factors of the second line. Here $\hat{C}_l^{(s)(f)a}$ and $\hat{C}_l^{(s)(f)b}$ denote cross-correlations between the CMB and foregrounds at frequency bands a and b, respectively. Note that these quantities vanish on an ensemble average, as CMB and foregrounds are uncorrelated with one another, i.e. $\langle C_l^{(s)(f)a}\rangle = 0 = \langle C_l^{(s)(f)b}\rangle$. However, for a particular realization these quantities need not vanish.

As mentioned above we make the estimate of bias in the power tensor assuming a single foreground component and two frequency channels. Thus, we find the empirical covariance matrix to be

$$\hat{\mathbf{C}}_l = \begin{pmatrix} \hat{C}_l^{(s)} + 2\hat{C}_l^{(s)(f)1} + C_l^{(f)1} & \hat{C}_l^{(s)} + \hat{C}_l^{(s)(f)1} + \hat{C}_l^{(s)(f)2} + C_l^{(f)1(f)2} \\ \hat{C}_l^{(s)} + \hat{C}_l^{(s)(f)1} + \hat{C}_l^{(s)(f)2} + C_l^{(f)1(f)2} & \hat{C}_l^{(s)} + 2\hat{C}_l^{(s)(f)2} + C_l^{(f)2} \end{pmatrix}. \tag{22}$$

Hence

$$\hat{\mathbf{C}}_l^{-1} = \frac{1}{\hat{\Delta}}\begin{pmatrix} \hat{C}_l^{(s)} + 2\hat{C}_l^{(s)(f)2} + C_l^{(f)2} & -\left(\hat{C}_l^{(s)} + \hat{C}_l^{(s)(f)1} + \hat{C}_l^{(s)(f)2} + C_l^{(f)1(f)2}\right) \\ -\left(\hat{C}_l^{(s)} + \hat{C}_l^{(s)(f)1} + \hat{C}_l^{(s)(f)2} + C_l^{(f)1(f)2}\right) & \hat{C}_l^{(s)} + 2\hat{C}_l^{(s)(f)1} + C_l^{(f)1} \end{pmatrix}, \tag{23}$$

where $\hat{\Delta}$ denotes the determinant of $\hat{\mathbf{C}}_l$. Using the above result we compute $\mathbf{e}_0^{\rm T}\hat{\mathbf{C}}_l^{-1}\mathbf{e}_0$ to get the cleaned map power spectrum as

$$\begin{aligned}\hat{C}_l^{\rm Clean} &= \frac{\hat{\Delta}}{C_l^{(f)1} + C_l^{(f)2} - 2C_l^{(f)1(f)2}} \\ &= \hat{C}_l^{(s)} + \frac{1}{\delta}\left[2\hat{C}_l^{(s)(f)1}C_l^{(f)2} + 2C_l^{(s)(f)2}\hat{C}_l^{(f)1} + C_l^{(f)1}C_l^{(f)2} - \left(C_l^{(f)1(f)2}\right)^2 - 2C_l^{(f)1(f)2}\left(\hat{C}_l^{(s)(f)1} + \hat{C}_l^{(s)(f)2}\right)\right. \\ &\quad \left. - \left(\hat{C}_l^{(s)(f)1}\right)^2 - \left(\hat{C}_l^{(s)(f)2}\right)^2 + 2\hat{C}_l^{(s)(f)1}\hat{C}_l^{(s)(f)2}\right], \end{aligned} \tag{24}$$

and the corresponding weights as

$$\begin{aligned}\hat{\mathbf{W}}_l &= \frac{\mathbf{e}_0^{\rm T}\hat{\mathbf{C}}_l^{-1}}{\mathbf{e}_0^{\rm T}\hat{\mathbf{C}}_l^{-1}\mathbf{e}_0} \\ &= \frac{1}{\delta}\begin{pmatrix} -\hat{C}_l^{(s)(f)1} + \hat{C}_l^{(s)(f)2} - C_l^{(f)1(f)2} + C_l^{(f)2} \\ \hat{C}_l^{(s)(f)1} - \hat{C}_l^{(s)(f)2} - C_l^{(f)1(f)2} + C_l^{(f)1} \end{pmatrix}. \end{aligned} \tag{25}$$

The symbol δ in the denominator of equation (24) and equation (25) is defined as $\delta = C_l^{(f)1} + C_l^{(f)2} - 2C_l^{(f)1(f)2}$. We next calculate all the terms in equation (20) one-by-one. First, consider the second term in the second line of equation (20):

$$a_{lm'}^{(s)}\hat{w}_l^{b'}a_{lm''}^{(f)b'*} = a_{lm'}^{(s)}\hat{w}_l^{1}a_{lm''}^{(f)1*} + a_{lm'}^{(s)}\hat{w}_l^{2}a_{lm''}^{(f)2*}. \tag{26}$$

Using equation (25) in equation (26) and then taking an ensemble average, we get

$$\left\langle a_{lm'}^{(s)}\hat{w}_l^{b'}a_{lm''}^{(f)b'*}\right\rangle = \frac{C_l^{(s)}}{(2l+1)\delta}\left[-a_{lm'}^{(f)1}a_{lm''}^{(f)1*} + a_{lm'}^{(f)1}a_{lm''}^{(f)2*} + a_{lm'}^{(f)2}a_{lm''}^{(f)1*} - a_{lm'}^{(f)2}a_{lm''}^{(f)2*}\right]. \tag{27}$$

To proceed further we assume that the foreground component follows rigid frequency scaling. We may parametrize the map of any foreground component at a frequency ν as

$$F(\hat{n}) = A_{\nu_0}(\hat{n})\left(\frac{\nu}{\nu_0}\right)^{-\beta(\hat{n})}, \tag{28}$$

where A_{ν_0} is the foreground template from observations made at a certain reference frequency ν_0 and its corresponding spectral index is $\beta(\hat{n})$. A foreground for which the approximation of a constant value of β over the entire sky holds is said to follow rigid frequency scaling, though,

© 2011 The Authors, MNRAS **414,** 1032–1046
Monthly Notices of the Royal Astronomical Society © 2011 RAS

Downloaded from https://academic.oup.com/mnras/article/414/2/1032/976641 by guest on 31 July 2023

in general β is a function of position on the sky, $\hat{n}$. In the case of a foreground for which the assumption of a constant spectral index may not hold, the deviations may be modelled with two terms each following the rigid scaling law (Bouchet & Gispert 1999). In that case,

$$F(\hat{n}) = A_{\nu_0}\left(\frac{\nu}{\nu_0}\right)^{-\overline{\beta}} + B_{\nu_0}(\hat{n})\left(\frac{\nu}{\nu_0}\right)^{-\overline{\beta}}\ln(\nu/\nu_0), \tag{29}$$

where $\overline{\beta}$ denotes mean spectral index of the foreground, $F(\hat{n})$, over the entire sky and A, B are two reference templates of $F(\hat{n})$. A very strong variation may require more than two templates for modelling.

Here, assuming a rigid scaling behaviour for the foreground component, we model the spectral coefficients of the foreground in a frequency band b as

$$a_{lm}^{(f)b} = A_{lm}\left(\frac{1}{f_b}\right)^{\alpha}. \tag{30}$$

Now, equation (27) becomes

$$\left\langle a_{lm'}^{(s)}\hat{w}_l^{b'}a_{lm''}^{(f)b'*}\right\rangle = -A_{lm'}A_{lm''}^{*}\frac{C_l^{(s)}}{(2l+1)\delta}\left(\frac{1}{f_1^{\alpha}}-\frac{1}{f_2^{\alpha}}\right)^2. \tag{31}$$

The third term after second equality in equation (20) is same as the second term. The fourth term is

$$\begin{aligned}\left\langle \hat{w}_l^b a_{lm'}^{(f)b}a_{lm''}^{(f)b'*}\hat{w}_l^{b'}\right\rangle &= \left\langle \left(\hat{w}_l^1 a_{lm'}^{(f)1}+\hat{w}_l^2 a_{lm'}^{(f)2}\right)\left(\hat{w}_l^1 a_{lm''}^{(f)1}+\hat{w}_l^2 a_{lm''}^{(f)2}\right)^*\right\rangle \\ &= \left\langle \left(\hat{w}_l^1\right)^2\right\rangle a_{lm'}^{(f)1}a_{lm''}^{(f)1*} + 2\left\langle \hat{w}_l^1\hat{w}_l^2\right\rangle a_{lm'}^{(f)1}a_{lm''}^{(f)2*} + \left\langle \left(\hat{w}_l^1\right)^2\right\rangle a_{lm'}^{(f)2}a_{lm''}^{(f)2*}.\end{aligned} \tag{32}$$

With rigid scaling approximation for the foreground and after some lengthy algebra, we finally get

$$\left\langle \hat{w}_l^b a_{lm'}^{(f)b}a_{lm''}^{(f)b'*}\hat{w}_l^{b'}\right\rangle = A_{lm'}A_{lm''}^{*}\frac{C_l^{(s)}}{(2l+1)\delta}\left(\frac{1}{f_1^{\alpha}}-\frac{1}{f_2^{\alpha}}\right)^2. \tag{33}$$

Here we have used

$$\delta = C_l^{(f)1}+C_l^{(f)2}-2C_l^{(f)1(f)2} = \frac{1}{2l+1}\sum_{m=-l}^{m=+l}|A_{lm}|^2\left(\frac{1}{f_1^{\alpha}}-\frac{1}{f_2^{\alpha}}\right)^2.$$

Finally we get, from equation (20),

$$\left\langle a_{lm'}^{\rm Clean}a_{lm''}^{\rm Clean*}\right\rangle = C_l^{(s)}\delta_{m'm''} - C_l^{(s)}A_{lm'}A_{lm''}^{*}\left(\sum_{m=-l}^{m=+l}|A_{lm}|^2\right)^{-1}. \tag{34}$$

Hence, we find that the low-l negative bias term leads to an anisotropic power tensor. As discussed in Saha et al. (2008) and Samal et al. (2010) this bias arises even in the case of perfect cleaning, where we have enough frequency channels to remove all the foregrounds. Besides this term, we also expect a positive contribution due to residual foreground contamination. This arises due to foregrounds which may not be eliminated by our cleaning procedure. By explicit numerical computation we find that the PEV of the power tensor corresponding to equation (34) is well aligned with the galactic poles. The other two orthogonal vectors of the power tensor lie in the galactic plane. This is of course expected since the eigenvectors are determined entirely by the galactic foregrounds, which are present predominantly along the galactic plane.

The main result of this section is that power tensor corresponding to the cleaned map acquires an anisotropic contribution due to low-l negative bias. This contribution arises even in the case of perfect cleaning when we have sufficient frequency channels to remove all the foregrounds present in the data. Although we have made several simplifying assumptions, this basic result is expected to hold in general. Our analytic results in this section, however, do not provide any guidance on how the PEV is affected due to foreground cleaning. In the next section, we estimate the total bias in the PEV by direct simulations.

4 RESULTS

4.1 Observational data

We first present the results from actual cosmological data and then discuss the simulation results. The PEVs, $\hat{n}_2$ and $\hat{n}_3$, for the quadrupole and octopole, respectively, from different clean maps extracted from the *WMAP* data are given in Table 1. The results presented here are for the *WMAP* ILC maps and the IPSE cleaned maps, with and without bias correction, for both 5- and 7-year data sets. All these maps are at resolution 9 of the HEALPIX sky tessellation format. The bias map, generated from Monte Carlo simulations of 500 random realizations, is shown in Fig. 1. The power spectrum corresponding to this bias map is shown in Fig. 2. As expected, we see that the bias correction is present, predominantly, in the galactic plane and is almost zero away from it. We point out that this bias is completely different from the negative bias discussed in the previous section.

The ILC map is obtained by linearly combining the temperature maps, observed in different frequency bands, in real space, with appropriate weights to remove the foregrounds. In contrast, the IPSE map is obtained by making linear combinations in harmonic space. We point out that the bias removal leads to a significantly improved cleaning in the galactic plane and has already been applied in the publicly

Downloaded from https://academic.oup.com/mnras/article/414/2/1032/976641 by guest on 31 July 2023

Table 1. The PEVs $\hat{n}_2$ and $\hat{n}_3$ of the quadrupole and octopole, respectively, for different clean maps.

	$\hat{n}_2$	$\hat{n}_3$
WMAP ILC map (5 year)	(0.2458, 0.4135, −0.8767)	(0.2505, 0.3823, −0.8895)
WMAP ILC map (7 year)	(0.2484, 0.3921, −0.8857)	(0.2434, 0.3842, −0.8906)
IPSE cleaned map (5 year)	(0.1481, 0.1923, −0.9701)	(0.2040, 0.3863, −0.8996)
Bias-corrected IPSE map (5 year)	(0.2936, 0.4091, −0.8640)	(0.2086, 0.3855, −0.8988)
IPSE cleaned map (7 year)	(0.1355, 0.1957, −0.9713)	(0.1782, 0.3773, −0.9088)
Bias-corrected IPSE map (7 year)	(0.2301, 0.3240, −0.9176)	(0.1773, 0.3754, −0.9097)

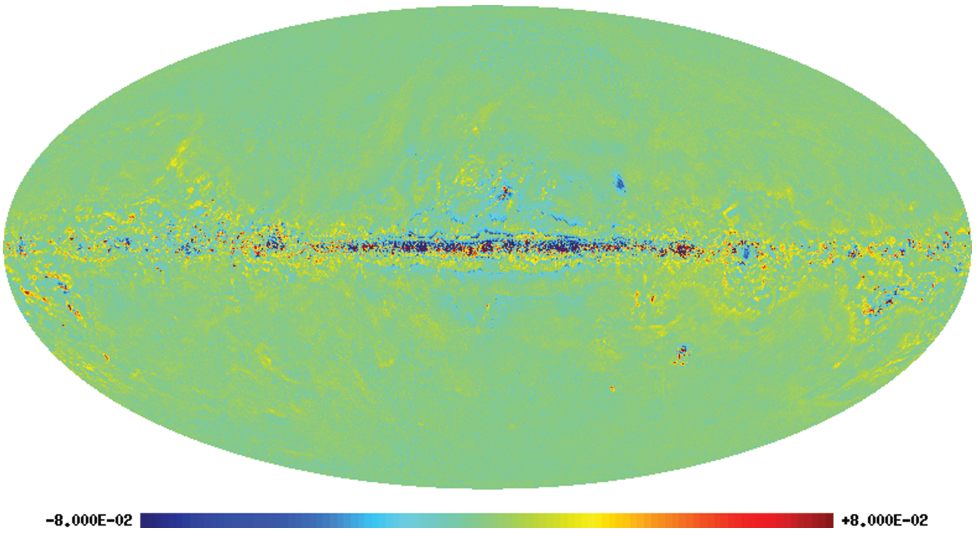

Figure 1. The bias-correction map, in units of μK, for 7-year data generated using the IPSE procedure with PSM for foregrounds (colour online).

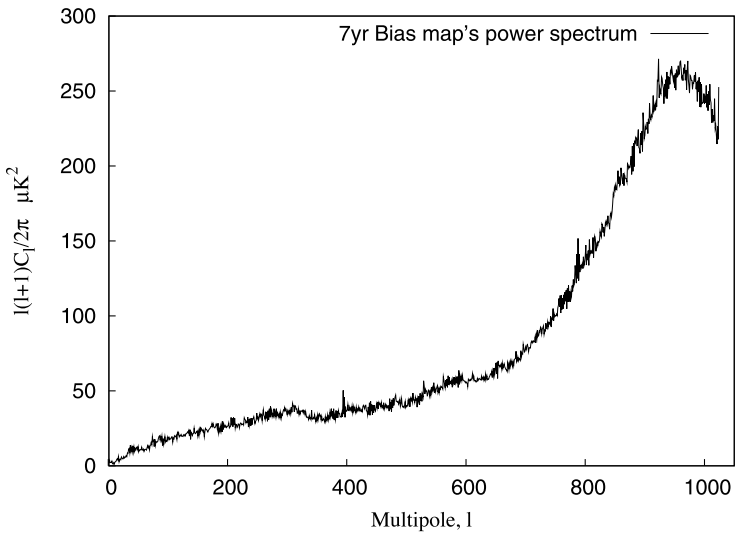

Figure 2. The power spectrum of the bias-correction map shown in Fig. 1.

available ILC map. The angle, $\delta\Theta$, between the two axes, $\hat{n}_2$ and $\hat{n}_3$, for different foreground cleaned maps, is listed in Table 2, along with an analytic estimate of probability that the observed alignment between these two PEVs in the *WMAP* data may be obtained as a random occurrence in an isotropic sample. This is given by $P = 1 - \hat{n}_2 \cdot \hat{n}_3 = 1 - \cos\delta\Theta$.

We find that the alignment between quadrupole and octopole is striking in both the ILC 5- and 7-year maps. We also note that, in the *WMAP* 3-year ILC map, the alignment of quadrupole and octopole is found to be 5°.87, which has a random occurrence probability of 0.00524. So, with more data release, the alignment appears to be getting better. The significance of the observed alignment in 7-year data is better than 4σ. The IPSE cleaned, bias-corrected 7-year map gives a significance better than 3σ. In comparison, the IPSE map without bias correction gives a much poorer alignment with $\delta\Theta = 11°.28$ [a 98.1 per cent confidence level (CL)]. The main difference between these two maps is

© 2011 The Authors, MNRAS **414,** 1032–1046
Monthly Notices of the Royal Astronomical Society © 2011 RAS

Downloaded from https://academic.oup.com/mnras/article/414/2/1032/976641 by guest on 31 July 2023

Table 2. The alignment angle $\delta\Theta$ between quadrupole and octopole in different foreground cleaned maps. Here $\delta\Theta$ is the angle between PEVs of quadrupole and octopole moments. Also listed are the analytic estimates of the probability that the observed alignment may arise in a random isotropic sample. This is given by $P = 1 - \hat{n}_2 \cdot \hat{n}_3 = 1 - \cos\delta\Theta$.

	$\delta\Theta$	$1 - \cos\delta\Theta$
WMAP ILC map (5 year)	1.°95	0.00058
WMAP ILC map (7 year)	0.°6	5.5×10^{-5}
IPSE cleaned map (5 year)	12.°27	0.023
Bias-corrected IPSE map (5 year)	5.°44	0.0045
IPSE cleaned map (7 year)	11.°28	0.019
Bias-corrected IPSE map (7 year)	4.°25	0.0027

that a significant foreground contamination in the galactic plane has been removed during the process of bias removal. This suggests that the effect of foregrounds is to distort the signal of alignment rather than to cause alignment.

We also notice from Table 1 that, as we remove the bias in the IPSE map, the octopole PEV changes only by a negligible amount, whereas the quadrupole PEV changed appreciably after applying bias correction. Indeed, after bias removal, the quadrupole PEV is relatively close to that corresponding to the ILC map. The IPSE octopole PEV agrees well with that obtained from the ILC map, irrespective of whether the bias is removed or not. So, it seems that quadrupole is more susceptible to distortion due to the presence of residual foregrounds.

4.2 Simulation results

We next use 500 simulated CMB maps to determine the effect of foreground cleaning on the properties of the extracted CMB signal. We find that 500 simulations are sufficient for most of the results obtained in this paper. The number of simulations is enlarged whenever necessary. The simulated maps containing CMB, foregrounds and detector noise are cleaned using the IPSE procedure. In each of the simulated maps, the bias due to foreground power in the galactic plane is removed in exactly the same manner as in the real data. Even after removing this bias, we expect that the PEV extracted from the cleaned map may not be exactly the same as that corresponding to the pure CMB map.

Let α be the angle between the pure map PEV ($\hat{n}_{\rm p}$) and cleaned map PEV ($\hat{n}_{\rm c}$) for a particular multipole. Here, we are interested only in the quadrupole and the octopole. We call this change in position of pure map PEVs as 'rotation' of PEVs in the presence of foregrounds. We want to find out whether there exists any preferred alignment of the pure map PEVs along a particular direction in the presence of foregrounds. In Fig. 3, we show the distribution of '$1 - \cos(\alpha)$', which is a convenient measure of the rotation of the PEVs. One can readily see from the graph that most of the PEVs do not undergo any significant shift. In fact, the number of PEVs that got rotated beyond a value of

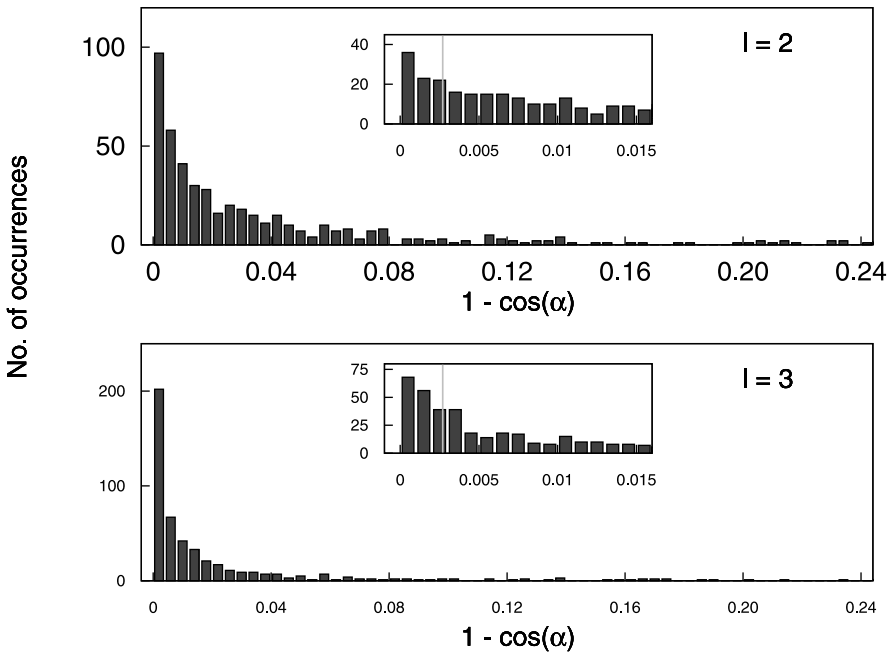

Figure 3. The distribution of $(1 - \cos\alpha)$, where α is the angle of rotation of pure maps PEVs in the presence of residual foregrounds. Here, the distribution of α is shown for both $l = 2$ (top) and $l = 3$ (bottom). The inset shows the range $0 < 1 - \cos\alpha < 0.015$ in more detail. The vertical line in the inset shows the level of alignment of multipoles $l = 2, 3$, $1 - \cos\delta\Theta = 0.0027$ for the 7-year IPSE bias-corrected map.

Downloaded from https://academic.oup.com/mnras/article/414/2/1032/976641 by guest on 31 July 2023

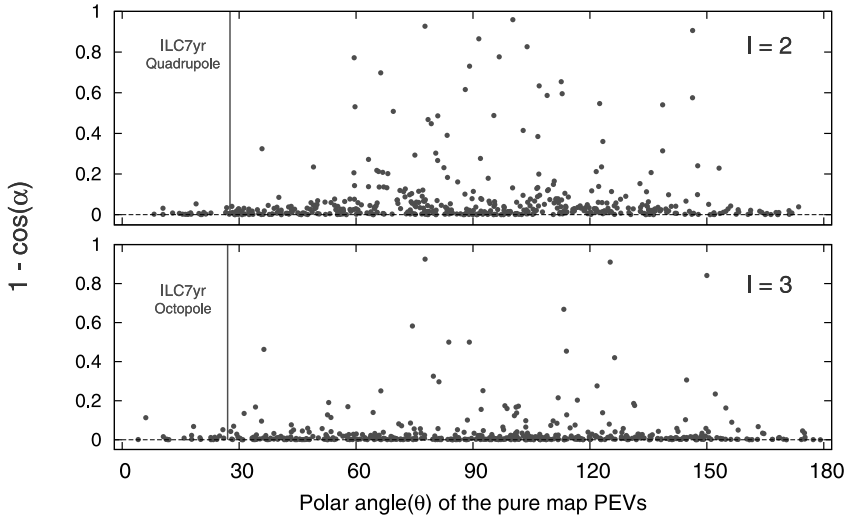

Figure 4. Plot of $(1 - \cos\alpha)$, as a function of polar angle, θ, of pure map PEVs. Here α is the rotation angle between the PEVs of pure CMB maps and bias-corrected clean maps. The vertical line indicates the polar angle of quadrupole (top) and octopole (bottom) PEVs of the *WMAP* 7-year ILC map.

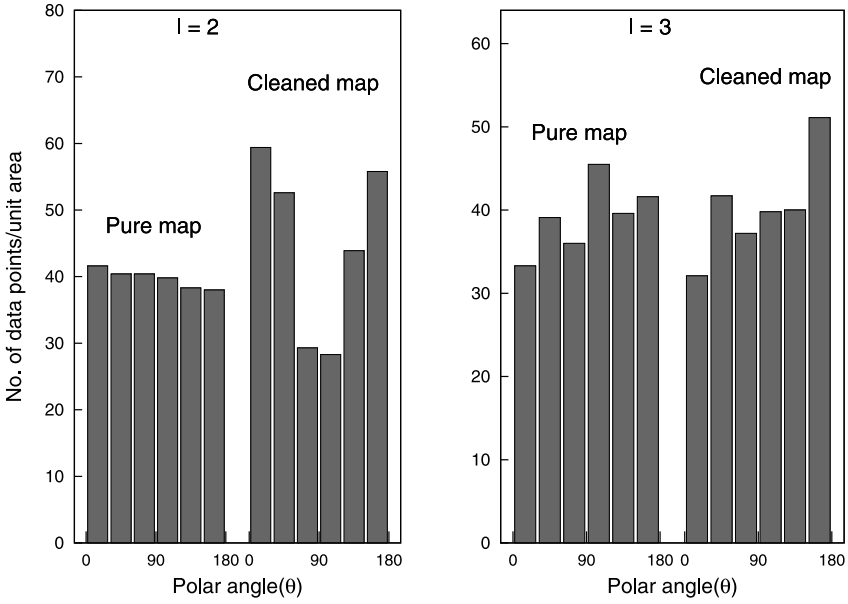

Figure 5. Distribution of the polar angle of PEVs in both the pure map and bias-corrected clean map ensembles for $l = 2, 3$. The dip at the centre in the $l = 2$ cleaned map indicates the tendency of PEVs to rotate away from the galactic plane in the presence of residual foregrounds. A similar dip is also present in the $l = 3$ cleaned map with much smaller amplitude.

$1 - \cos(\alpha) = 0.15$ is 52 for $l = 2$, and 30 for $l = 3$, out of the 500 bias-corrected clean maps. Hence, the error introduced due to foregrounds on the extraction of the PEVs is generally small.

Fig. 4 shows the plot of '$1 - \cos(\alpha)$', for all the 500 simulated maps, as a function of the polar angle, θ, of the pure map PEV, for both $l = 2$ and 3. Notice the clustering of data points near the zero of the y-axis in this plot, which indicates only a very nominal shift in most of the PEVs. It also shows that the PEVs which were lying, initially, in the galactic plane generally undergo larger rotation whereas the effect is small on PEVs at higher latitudes. Note that the galactic foregrounds extend roughly up to 30° on either side of the galactic equator and are distributed asymmetrically. Next, in Fig. 5 we show the distribution of PEVs in different sky regions for $l = 2$ and 3. The histograms are shown for both pure and cleaned maps in an interval of 30° of polar angle across the sky. The distribution of pure map PEVs is relatively flat, as expected. However, the foreground cleaned maps show a dip near the galactic plane. This illustrates that in the cleaned maps the PEVs have a tendency to rotate away from the galactic plane. This effect is seen to be more pronounced in the case of the quadrupole in comparison to the octopole. The effect is easily understood since the region of the galactic plane is most contaminated by foregrounds. Hence the PEVs in the galactic plane are naturally expected to undergo larger rotation.

Next, we look at the alignment of quadrupole and octople in both pure and cleaned maps. Fig. 6 shows the distribution of '$1 - \cos(\alpha_{23})$', where α_{23} is the angle between the quadrupole and the octopole. The data are binned with a bin size of 0.2. We can

© 2011 The Authors, MNRAS **414,** 1032–1046
Monthly Notices of the Royal Astronomical Society © 2011 RAS

Downloaded from https://academic.oup.com/mnras/article/414/2/1032/976641 by guest on 31 July 2023

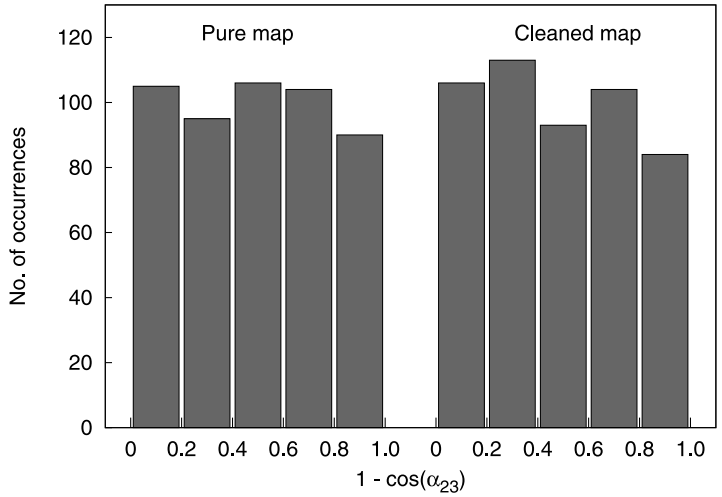

Figure 6. Distribution of $1 - \cos(\alpha_{23})$ where α_{23} is the angle between the quadrupole and octopole. Results are shown for both the pure maps and bias-corrected clean maps. The distribution is found to be very close to uniform in both cases, indicating isotropy.

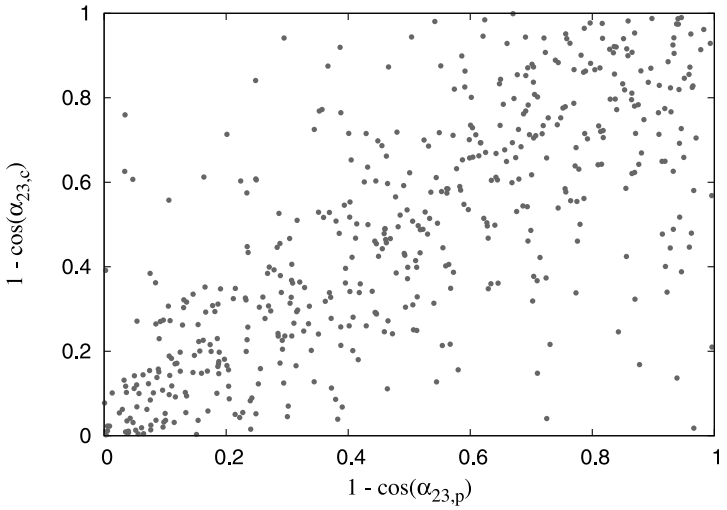

Figure 7. The alignment between quadrupole and octopole of pure map and bias-corrected clean maps. On the *y*-axis, we have $1 - \cos(\alpha_{23,c})$, where $\cos\alpha_{23,c} = \hat{n}_{l2} \cdot \hat{n}_{l3}$, and $\hat{n}_{l2}$ and $\hat{n}_{l3}$ are the PEVs corresponding to $l = 2$ and 3, respectively, for the simulated foreground cleaned maps. On the *x*-axis, we have the same measure corresponding to the pure CMB maps. No preferred alignment was seen in the simulated maps.

easily infer from the figure that these alignments are completely random. Hence, we find no evidence for foreground induced alignment in the cleaned maps. In Fig. 7 we show a plot of $1 - \cos(\alpha_{23,p})$ versus $1 - \cos(\alpha_{23,c})$ for all the 500 simulations. Here, the subscripts 'p' and 'c' stand for 'pure' and 'clean' simulated CMB maps, respectively. If there is any correlation it will show up in such a plot. However, this plot illustrates that there is no sign of preferred alignment.

We next compute the *P* value or the probability that the alignment seen in data arises due to a random fluctuation directly from simulations. We determine the number of random realizations of CMB data which show better alignment in comparison to what is observed in *WMAP* data. The probability is obtained by dividing this number by the total number of random samples. Here we use both the randomly generated pure CMB maps as well as simulated foreground cleaned maps. For the bias-corrected IPSE 5-year map we find that the probability is 0.004 if we use the simulated pure CMB maps. The probability remains unchanged if it is computed by using the simulated cleaned maps. The corresponding numbers for the 7-year maps are 0.004 and 0.002 for the simulated pure CMB maps and the cleaned maps, respectively. The result remains unchanged if we apply the residual foreground bias correction to the simulated cleaned maps. These results have been obtained by using 500 simulations. For a signal of alignment at a CL of 3σ, seen in the IPSE bias-corrected map, we need at least $1/(1 - 0.997) \approx 333$ number of random realizations of CMB sky. A 500 maps ensemble that we generated here for our study is barely sufficient to test the alignment at 99.7 per cent CL. Hence we verified these results by using an additional 500 simulations. These did not lead to any significant change in results. The simulation results agree well with those given in Table 2.

As we have mentioned earlier, the negative bias does cause a systematic reduction of power for low-*l* multipoles. This is seen clearly in Fig. 8 where we plot the sum of the eigenvalues of the power tensor for $l = 2$, 3 for both simulated pure and bias-corrected clean maps. The sum of eigenvalues equals the total power, C_l, in each multipole. We find a systematic negative shift in the power in each of the cleaned maps.

Downloaded from https://academic.oup.com/mnras/article/414/2/1032/976641 by guest on 31 July 2023

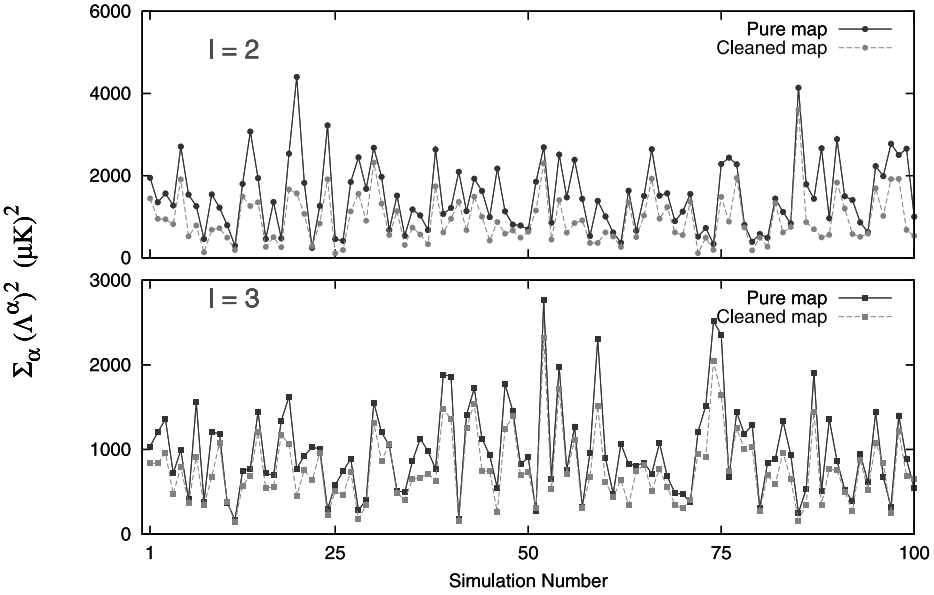

Figure 8. The sum of eigenvalues or the total power, C_l, for $l = 2$, 3 of the simulated pure and cleaned CMB maps, after bias correction. We see a systematic negative shift in the power in each of the simulated clean maps.

After taking the average over all the simulations, we find that quadrupole power of the cleaned map is lower by 39 per cent in comparison to that of the pure CMB map. The corresponding octopole power gets reduced by 22 per cent.

To summarize, we find no evidence for any systematic effect which may cause alignment of PEVs, despite the presence of a systematic effect on power, C_l. We do find a systematic shift of the PEVs away from the galactic plane. However, the final PEVs point in random directions. Hence, rather than causing alignment, this effect has a tendency to distort any signal of alignment that might be present in the original sample.

Our results strongly suggest that the alignment is caused by some effect other than foreground contamination. The foregrounds lead to a random shift in the PEVs causing a certain level of misalignment. Hence the angle between $l = 2$ and 3 PEVs must not be very small in comparison to the shift caused by foregrounds. The shift of the PEVs is quantified by the distribution plot shown in Fig. 3. This should be associated with the randomness that the cleaning process introduces in the extraction of the PEVs. We find that the probabilities of chance alignment for the IPSE cleaned 5- and 7-year maps, after bias correction, are 0.0045 and 0.0027, respectively. We find that about 16 per cent of the simulations have $(1 - \cos\alpha) < 0.0027$. At high galactic latitudes, corresponding to the Virgo alignment axis, this number is higher. It is reassuring that the number of random samples which show a shift in the PEV less than the observed alignment in the IPSE cleaned map is not too small.

4.3 Subdominant foreground components

So far we have only considered the dominant components of the foregrounds in our analysis. We next briefly address the issue of subdominant foregrounds. The known subdominant foregrounds are described in Section 2.3. As discussed in Section 2.3, there is considerable uncertainty in these components and a reliable model over the entire sky is not available.

Our analysis suggests that the foreground cleaning really tends to distort any signal of alignment rather than causing alignment. The only systematic trend we have seen so far is a shift away from the galactic equatorial plane. The shift is larger for $l = 2$ and much smaller for $l = 3$. Hence it tends to cause misalignment rather than alignment. The only way this can cause alignment is if the foreground level is so large that both $l = 2$, 3 get pushed towards the galactic poles. However, the level of foregrounds required for this is unrealistically large. Subdominant foregrounds of the type discussed in Section 2.3 cannot produce such an effect. In order to produce an alignment in the direction of Virgo, as seen in data, we would require an unrealistically large foreground component in a plane perpendicular to the PEV corresponding to $l =$ 2, 3 seen in data. The level of foreground required for this purpose would be much larger than even the galactic foregrounds. Hence such a scenario is ruled out.

In order to explicitly check the effect of subdominant foregrounds we added some additional foregrounds at random. Their strength was chosen to be less than 20 per cent of the dominant foregrounds. We also added a foreground component along the supercluster plane and separately in a patch of angular size $20^\circ \times 20^\circ$ in the direction of the PEV corresponding to $l = 2$, 3. These foregrounds are chosen to be well correlated with the direction of the observed axis of alignment in the *WMAP* data. Hence they have the best chance of causing alignment in the simulated data sets. The spectral index in these cases was chosen to be different from that of the dominant foregrounds. No change in results was detected in any of these studies. The random simulations did not show any evidence for alignment of the $l = 2$, 3 multipoles.

© 2011 The Authors, MNRAS **414,** 1032–1046
Monthly Notices of the Royal Astronomical Society © 2011 RAS

Downloaded from https://academic.oup.com/mnras/article/414/2/1032/976641 by guest on 31 July 2023

The results and discussion in this section clearly suggest that even unknown subdominant foregrounds are unlikely to change the main results of our paper. It is highly inconceivable that they can cause alignment as long as their strength is a fraction of the dominant foregrounds. We postpone an exhaustive study of such foregrounds for future research.

5 CONCLUSIONS

We have studied the effect of foreground cleaning on the alignment of low-l multipoles, $l = 2, 3$. It has been speculated in the past that the alignment may be caused by foreground contamination. The presence of residual foreground power in the cleaned CMB maps could lead to violation of statistical isotropy and hence alignment of low-l multipoles. Furthermore, even in the case of perfect cleaning, the extracted power contains a negative bias, which is quite significant at low l. This has been shown explicitly in the case of the IPSE procedure and in the ILC map (Chiang, Naselsky & Coles 2008). Using the IPSE procedure, we analytically compute the power tensor using some simplifying assumptions. We find that its ensemble average is not proportional to an identity matrix due to the presence of low-l bias. Hence this implies a violation of statistical isotropy. We next performed detailed numerical simulations within the framework of the IPSE method to determine the effect of foregrounds on the observed alignment.

Our IPSE simulation results, obtained using 500 randomly generated samples, show that the PEVs extracted from foreground cleaned maps are generally in good agreement with those obtained from pure CMB maps. In most cases the shift in PEVs is observed to be small. The largest change is seen in the case of the quadrupole. The shift is dominant for PEVs which initially lie close to the galactic plane. In general, we find that the PEVs tend to get pushed away from the galactic plane towards the galactic poles. A similar trend is also seen in the case of the octopole but with much reduced significance. We do not, however, see any evidence for alignment among the quadrupole and octopole PEVs in the foreground reduced maps. The significance or P values extracted by using simulated clean maps are found to be in good agreement with those obtained by using simulated pure CMB maps. These also show good agreement with the results obtained analytically and listed in Table 2.

Hence, despite the systematic shift of PEVs away from the galactic plane, as observed dominantly in the case of the quadrupole, we find that foregrounds do not cause alignment of quadrupole and octopole. This is because the change in PEVs due to foreground cleaning is generally small and mostly in random directions. One might be tempted to propose a scenario where the shift towards galactic poles is a much more significant effect which may be caused by the presence of a much stronger level of foreground contamination. In this case it is conceivable that the PEVs extracted from the foreground cleaned maps would point dominantly towards the galactic poles and hence show alignment. However, this would require a very large foreground contamination in comparison to the currently accepted model. The level of contamination has to be sufficiently large so that both the quadrupole and octopole PEVs tend to align with the galactic poles. Although the quadrupole shows a somewhat significant shift of PEVs away from galactic plane, this trend is barely notable in the case of the octopole. We emphasize that even in the case of the quadrupole the shift of PEV is very small in most cases. Furthermore, such a proposal will imply that the direction of alignment points towards the galactic poles which is not consistent with the observed axis. Hence we infer that foreground contamination is very unlikely to cause the observed alignment.

A significant effect is observed in the case of total power, C_l, for low-l multipoles. We see a systematic cut-off of power in these multipoles which has been attributed to a chance correlation of CMB signal and residual foregrounds. Since such a systematic trend in alignment is not observed, we conclude that the observed alignment and anomalously low power may be independent of each other.

Because of the random nature of the shift caused by foreground cleaning, it is more likely to cause misalignment of multipoles. We see this clearly by comparing the results from IPSE cleaned maps, before and after removing the bias due to foreground contamination in the galactic plane. The alignment is found to be much stronger after removing the residual foreground bias which arises due to remnant foregrounds present in our cleaned maps. Furthermore, we see that alignment becomes much more significant as more data are accumulated. The alignment seen in 7-year data, for example, is much better than seen in 5-year data which in turn is better than that seen in 3-year data. This is clearly caused by reduced uncertainties as more data accumulate. Hence, we conclude that both the foregrounds and detector noise are more likely to distort, rather than cause alignment.

ACKNOWLEDGMENTS

We acknowledge the use of the Legacy Archive for Microwave Background Data Analysis. Some of the results of this work are derived using the publicly available HEALPIX package (Górski et al. 2005). (The HEALPIX distribution is publicly available from the website http://healpix.jpl.nasa.gov.) We acknowledge the use of the *Planck* Sky Model, developed by the Component Separation Working Group (WG2) of the *Planck* Collaboration. PKA thanks the Council of Scientific and Industrial Research (CSIR), India, for providing his PhD fellowship. His fellowship number is F.No.09/092(0413)/2005-EMR-I. PKS thanks NISER, Bhubaneswar, for providing their computer and library facility. We thank Rajib Saha for useful discussions. We thank Adrian Chapman for discussions and for collaboration in the analysis of subdominant foregrounds.

REFERENCES

Abramo L. R., Sodre L., Jr, Wuensche C. A., 2006, Phys. Rev. D, 74, 083515
Ackerman L., Carroll S. M., Wise M. B., 2007, Phys. Rev. D, 75, 083502

Downloaded from https://academic.oup.com/mnras/article/414/2/1032/976641 by guest on 31 July 2023

Armendariz-Picon C., 2004, J. Cosmol. Astropart. Phys., 7, 7
Battye R. A., Moss A., 2006, Phys. Rev. D, 74, 041301
Bennett C. L. et al., 2003a, ApJS, 148, 1
Bennett C. L. et al., 2003b, ApJS, 148, 97
Berera A., Buniy R. V., Kephart T. W., 2004, J. Cosmol. Astropart. Phys., 10, 16
Bernui A., Villela T., Wuensche C. A., Leonardi R., Ferreira I., 2006, A&A, 454, 409
Bernui A., Mota B., Reboucas M. J., Tavakol R., 2007, A&A, 464, 479
Bielewicz P., Górski K. M., Banday A. J., 2004, MNRAS, 355, 1283
Bielewicz P., Eriksen H. K., Banday A. J., Górski K. M., Lilje P. B., 2005, ApJ, 635, 750
Birch P., 1982, Nat, 298, 451
Bonaldi A., Ricciardi S., Leach S., Stivoli F., Baccigalupi C., de Zotti G., 2007, MNRAS, 382, 1791
Bouchet F. R., Gispert R., 1999, New Astron., 4, 443
Buniy R. V., Berera A., Kephart T. W., 2006, Phys. Rev. D, 73, 063529
Carroll S. M., Tseng C.-Y., Wise M. B., 2010, Phys. Rev. D, 81, 083501
Chiang L.-Y., Naselsky P. D., Coles P., 2008, Modern Phys. Lett. A, 23, 1489
Copi C. J., Huterer D., Schwarz D. J., Starkman G. D., 2006, MNRAS, 367, 79
Copi C. J., Huterer D., Schwarz D. J., Starkman G. D., 2007, Phys. Rev. D, 75, 023507
Cruz M., Martinez-Gonzalez E., Vielva P., Cayon L., 2005, MNRAS, 356, 29
Delabrouille J., Cardoso J. F., 2009, in Martínez V. J., Saar E., Martínez-González E., Pons-Bordería M.-J., eds, Lecture Notes in Physics 665, Data Analysis in Cosmology. Springer-Verlag, Berlin, p. 159
de Oliveira-Costa A., Tegmark M., 2006, Phys. Rev. D, 74, 023005
de Oliveira-Costa A. et al., 2002, ApJ, 567, 363
de Oliveira-Costa A., Tegmark M., Zaldarriaga M., Hamilton A., 2004, Phys. Rev. D, 69, 063516
Diego J. M., Cruz M., González-Nuevo J., Maris M., Ascasibar Y., Burigana C., 2010, MNRAS, 402, 1213
Dobler G., Finkbeiner D. P., 2008a, ApJ, 680, 1222
Dobler G., Finkbeiner D. P., 2008b, ApJ, 680, 1235
Erickcek A. L., Hirata C. M., Kamionkowski M., 2009, Phys. Rev. D, 80, 083507
Eriksen H. K., Hansen F. K., Banday A. J., Górski K. M., Lilje P. B., 2004, ApJ, 605, 14
Eriksen H. K. et al., 2007a, ApJ, 656, 641
Eriksen H. K., Banday A. J., Górski K. M., Hansen F. K., Lilje P. B., 2007b, ApJ, 660, L81
Eriksen H. K., Jewell J. B., Dickinson C., Banday A. J., Górski K. M., Lawrence C. R., 2008, ApJ, 676, 10
Freeman P. E., Genovese C. R., Miller C. J., Nichol R. C., Wasserman L., 2006, ApJ, 638, 1
Gold B. et al., 2009, ApJS, 180, 265
Gold B. et al., 2011, ApJS, 192, 15
Gordon C., Hu W., Huterer D., Crawford T., 2005, Phys. Rev. D, 72, 103002
Górski K. M., Hivon E., Banday A. J., Wandelt B. D., Hansen F. K., Reinecke M., Bartelmann M., 2005, ApJ, 622, 759
Gruppuso A., Burigana C., 2009, J. Cosmol. Astropart. Phys., 08, 004
Gruppuso A., Burigana C., Finelli F., 2007, MNRAS, 376, 907
Hajian A., Souradeep T., 2006, Phys. Rev. D, 74, 123521
Hajian A., Souradeep T., Cornish N., 2004, ApJ, 618, L63
Hansen F. K., Banday A. J., Górski K. M., 2004, MNRAS, 354, 641
Hansen F. K., Banday A. J., Eriksen H. K., Górski K. M., Lilje P. B., 2006, ApJ, 648, 784
Hansen F. K., Banday A. J., Górski K. M., Eriksen H. K., Lilje P. B., 2009, ApJ, 704, 1448
Haslam C. G. T., Salter C. J., Stoffel H., Wilson W. E., 1982, A&AS, 47, 1
Helling R. C., Schupp P., Tesileanu T., 2006, Phys. Rev. D, 74, 063004
Hill R. S. et al., 2009, ApJS, 180, 246
Hinshaw G. et al., 2007, ApJS, 170, 288
Hoftuft J., Eriksen H. K., Banday A. J., Górski K. M., Hansen F. K., Lilje P. B., 2009, ApJ, 699, 985
Hutsemékers D., 1998, A&A, 332, 410
Hutsemékers D., Lamy H., 2001, A&A, 367, 381
Inoue K. T., Silk J., 2006, ApJ, 648, 23
Itoh Y., Yahata K., Takada M., 2010, Phys. Rev. D, 82, 043530
Jain P., Ralston J. P., 1999, Modern Phys. Lett. A, 14, 417
Jain P., Narain G., Sarala S., 2004, MNRAS, 347, 394
Kahniashvili T., Lavrelashvili G., Ratra B., 2008, Phys. Rev. D, 78, 063012
Kashlinsky A., Atrio-Barandela F., Kocevski D., Ebeling H., 2008, ApJ, 686, L49
Kashlinsky A., Atrio-Barandela F., Kocevski D., Ebeling H., 2009, ApJ, 691, 1479
Katz G., Weeks J., 2004, Phys. Rev. D, 70, 063527
Kogut A., Banday A. J., Bennett C. L., Gorski K. M., Hinshaw G., Smoot G. F., Wright E. I., 1996, ApJ, 464, L5
Koivisto T., Mota D. F., 2008, ApJ, 679, 1
Lamarre J.-M. et al., 2010, A&A, 520, A9
Land K., Magueijo J., 2006, MNRAS, 367, 1714
Land K., Magueijo J., 2007, MNRAS, 378, 153
La Porta L., Burigana C., Reich W., Reich P., 2008, A&A, 479, 641
Leach S. M. et al., 2008, A&A, 491, 597
Magueijo J., Sorkin R. D., 2007, MNRAS, 377, L39
Maino D. et al., 2002, MNRAS, 334, 53
Mandolesi N. et al., 2010, A&A, 520, A3

Downloaded from https://academic.oup.com/mnras/article/414/2/1032/976641 by guest on 31 July 2023

Martínez-González E., Diego J. M., Vielva P., Silk J., 2003, MNRAS, 345, 1101
Moffat J. W., 2005, J. Cosmol. Astropart. Phys., 10, 12
Naselsky P. D., Verkhodanov O. V., Nielsen M. T. B., 2008, Astrophys. Bull., 63, 216
Planck Collaboration, 2005, Planck Blue Book. The Scientific Programme, Planck Collaboration, ESA Publication, ESA-SCI(2005)01
Prunet S., Uzan J.-P., Bernardeau F., Brunier T., 2005, Phys. Rev. D, 71, 083508
Rakić A., Schwarz D. J., 2007, Phys. Rev. D, 75, 103002
Rakić A., Rasanen S., Schwarz D. J., 2006, MNRAS, 369, L27
Ralston J. P., Jain P., 2004, Int. J. Modern Phys. D, 13, 1857
Reich W., Reich P., 2008, Proc. Int. Astron. Union, 4, 603
Rodrigues D. C., 2008, Phys. Rev. D, 77, 023534
Saha R., Jain P., Souradeep T., 2006, ApJ, 645, L89
Saha R., Prunet S., Jain P., Souradeep T., 2008, Phys. Rev. D, 78, 023003
Samal P. K., Saha R., Jain P., Ralston J. P., 2008, MNRAS, 385, 1718
Samal P. K., Saha R., Jain P., Ralston J. P., 2009, MNRAS, 396, 511
Samal P. K., Saha R., Delabrouille J., Prunet S., Souradeep T., 2010, ApJ, 714, 840
Sarkar D., Huterer D., Copi C. J., Starkman G. D., Schwarz D. J., 2010, preprint (arXiv:1004.3784)
Schwarz D. J., Starkman G. D., Huterer D., Copi C. J., 2004, Phys. Rev. Lett., 93, 221301
Slosar A., Seljak U., 2004, Phys. Rev. D, 70, 083002
Tauber J. A. et al., 2010, A&A, 520, A1
Tegmark M., Efstathiou G., 1996, MNRAS, 281, 1297
Tegmark M., de Oliveira-Costa A., Hamilton A. J., 2003, Phys. Rev. D, 68, 123523
Vielva P., Wiaux Y., Martinez-Gonzalez E., Vandergheynst P., 2007, MNRAS, 381, 932
Wiaux Y., Vielva P., Martinez-Gonzalez E., Vandergheynst P., 2006, Phys. Rev. Lett., 96, 151303

This paper has been typeset from a TEX/LATEX file prepared by the author.

Downloaded from https://academic.oup.com/mnras/article/414/2/1032/976641 by guest on 31 July 2023